Wideband Impedance Passivation of MMCs for Suppressing Harmonic Oscillations

Pengxiang Huang, *Member, IEEE*, and Heng Wu, *Senior Member, IEEE*, and Luigi Vanfretti, *Senior Member, IEEE*, and Oriol Gomis-Bellmunt, *Fellow, IEEE*

***Abstract*—Harmonic instability and associated oscillation events have become one of the main concerns in MMC-based HVdc systems. These oscillations can appear in the range from a few hundred hertz to several kilohertz, and the root cause is identified as delay-induced negative damping of MMC impedance appearing at the system resonance frequency. This paper introduces a wideband impedance reshaping method through MMC control to eliminate such negative damping for both grid-following (GFL) and grid-forming (GFM) MMCs, which makes the MMC impedance completely passive from the second harmonic frequency upward, thus preventing all harmonic oscillations. First, simplified impedance models of MMCs are derived for the harmonic stability analysis and the impedance reshaping control design. Next, a passivity-based impedance reshaping method is presented, as well as practical considerations for its implementation. In addition, to maintain the MMC's disturbance ride-through capability, an adaptive activation scheme is developed, which enables the wideband impedance reshaping control only in the presence of harmonic oscillation events. The effectiveness of the proposed method is validated by frequency domain analysis and by electromagnetic transient (EMT) simulations of two typical MMC-based power systems.**

***Index Terms*—MMC, impedance-based stability, passivity, active damping, adaptive control**

I. Introduction

MODULAR multilevel converter (MMC)-based high voltage dc (HVdc) transmission systems have been broadly developed in the past decade, aiming to improve the efficiency and reliability in transferring large amounts of electricity. Similar to type-III/type-IV turbines [1], MMCs are prone to oscillation issues when connected to ac systems. Oscillations of MMC in the low-frequency range (i.e., near-synchronous range) have been widely observed and studied for more than a decade, as reported in [2], [3] and [4]. In the last few years, a new type of oscillation event, beyond the low-frequency range, has been widely reported in several MMC-based HVdc projects. Examples of this new oscillation event include: 1) a $\sim$ 1700 Hz oscillation on both sides of the INELFE HVdc link in France [5]; 2) a 1271 Hz oscillation between the Lu'xi side MMC and a long overhead transmission line (OTL) in China [6]; 3) a 1810 Hz oscillation at the Hu'bei side MMC and a 695 Hz oscillation at the Chong'qing side MMC in the Yu'e back-to-back HVdc project in China [7]; and 4) a 320 Hz and 2000 $\sim$ 2500 oscillations between the offshore MMC and wind farm in Ru'dong in China [8], [9]. The frequencies of these oscillations are all above the second harmonic frequency, and the root cause of the oscillation has been attributed to the system resonance that falls into the negative damping region of the MMC impedance induced by time delay [10], [11]. Therefore, it is necessary to develop a method to eliminate such delay-induced negative damping of MMCs. According to the passivity-based controller design presented in [10], oscillation of a converter can be prevented by reshaping the converter impedance to have a non-negative real-part at system resonance frequencies. This can be achieved in different ways when applied to MMC: 1) tuning the parameters of existing control functions [12]; 2) applying a cascading low-pass filter [6], [7] or a notch filter [13], [14] with existing control functions to counteract the time delay effect in certain frequency range; and 3) employing supplementary control schemes to compensate for negative damping [15], [16]. All these methods incorporate active control functions, which are susceptible to time delay impact as existing controls. As a result, except for narrowband methods in [13]–[15], all other methods share a common challenge: the time delay effect is difficult to compensate for over a wide frequency range, and it will inevitably add phase lag to reshaping functions (i.e.,damping control function). This delay-related phase shift, when coupled with the inherent phase shift of the wideband control function (e.g., phase shift of a low-pass filter in its transition band and passband), can easily lead to an increase of the negative damping of MMC in certain frequency ranges. In addition, these wideband functions may interfere with existing control functions, potentially deteriorating transient performance and controller stability of MMC. To address the issues mentioned above, the wideband impedance reshaping method outlined in [17] deactivates the feedback structure of the existing control loop and reconstructs the reference tracking functionality by inserting a specially designed transfer function into the forward path of the existing control loop. By shaping the MMC impedance as a pure inductance, this technique ensures that the resulting MMC impedance has a nonnegative real part across a frequency range from 200 Hz to the Nyquist frequency. However, except for still leaving a small amount of negative damping in hundred hertz range, such method also causes a reduced dynamics under voltage disturbance, which deteriorates the MMC's disturbance ride-

This work was authored in part by the National Renewable Energy Laboratory, operated by Alliance for Sustainable Energy, LLC, for the U.S. Department of Energy (DOE) under Contract No. DE-AC36-08GO28308. Funding provided by U.S. Department of Energy Office of Energy Efficiency and Renewable Energy Wind Energy Technologies Office. The views expressed in the article do not necessarily represent the views of the DOE or the U.S. Government. The U.S. Government retains and the publisher, by accepting the article for publication, acknowledges that the U.S. Government retains a nonexclusive, paid-up, irrevocable, worldwide license to publish or reproduce the published form of this work, or allow others to do so, for U.S. Government purposes.

through capabilities. In addition, modifying vendor-specific control designs is usually complex, even impossible, and could lead to other unexpected operational issues.

In contrast to the wideband approach, the narrowband methods proposed in [13] and [15] can selectively and narrowly eliminate negative damping around the intended frequencies, without affecting the dynamics and stability of existing controls. However, implementing narrowband damping control demands complicated design considerations to fine-tune the damping gain and the width of damping band, especially when targeting multiple oscillation frequencies simultaneously. Moreover, to guarantee effectiveness of damping, the narrowband methods require the use of online algorithms that identify oscillation frequencies and adjust damping functions according to changes in system resonance conditions. Any inaccuracies in the estimation of the oscillation frequency and the adjustment of damping functions can lead to unintended consequences at and near the intended frequency, potentially introducing new instability problems (as elaborated in [18]).

To overcome the challenges of existing impedance reshaping methods, this work introduces a passivity-based wideband impedance reshaping control method, named 'wideband passivation'. This method can effectively eliminate delay-induced negative damping of the GFL-/GFM-MMC impedance from the second harmonic frequency upwards, with its efficacy remaining independent of the amount of delay. It functions by adding a supplementary damping control loop in parallel with existing controls, thereby preserving the desired transient performance and stability of existing controllers. To maintain the MMC's disturbance ride-through capability, an online oscillation detection-based adaptive control scheme is also proposed in this article. This provides a plug-and-play solution, ensuring that the proposed wideband passivation loop is activated only when oscillatory events are detected.

The remainder of the paper is organized as follows. Section II describes a typical structure of an MMC-based power system and derives the simplified impedance model for grid-following (GFL) and grid-forming (GFM) MMCs, which can be used for harmonic stability analysis, as well as the design of the wideband passivation method in the sequel. Section III presents a passivity-based design principle for developing wideband passivation loops for GFL-MMC and GFM-MMC, details on practical implementation are given as well. Section IV proposes an adaptive strategy to reshape the impedance through the proposed wideband passivation. Section V verifies the effectiveness of the proposed wideband passivation method by performing frequency domain impedance scans and conducting EMT simulations of two typical MMC-based systems. Section VI concludes this paper.

II. MMC and System Description

A. Overall System Description

Figure 1 presents a simplified schematic of a MMC-based system, which also indicates how the proposed wideband passivation loop should be introduced. Note that, it includes an online oscillation dectection unit that adaptively activates the passivation loop based on the monitoring of system stability

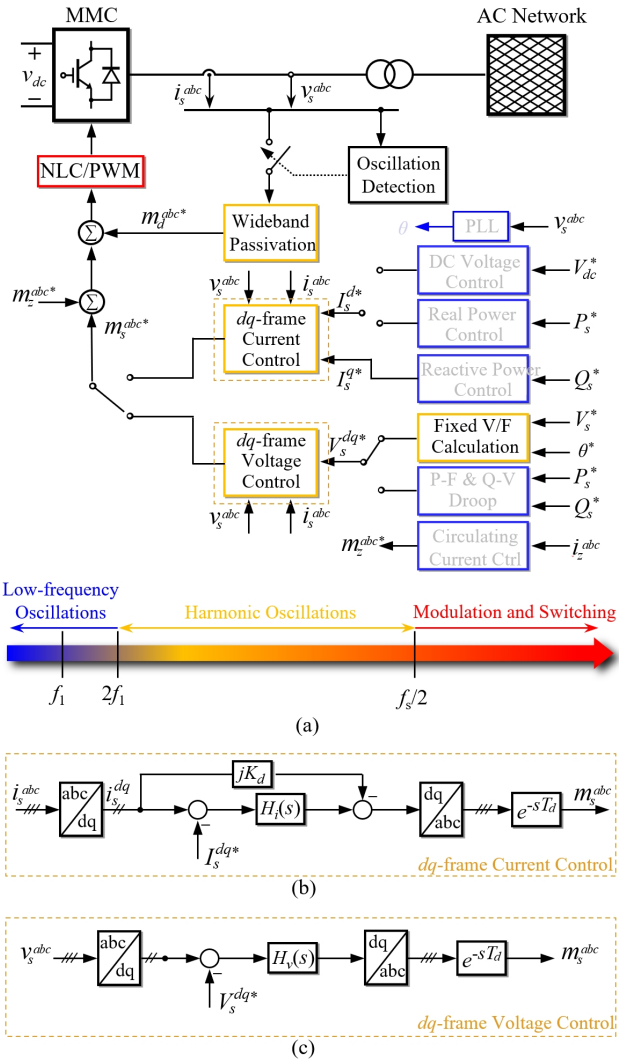

Fig. 1. (a) Control schems of MMC and its mapping to different forms of oscillations; (b) ac current control in dq-reference frame; (c) ac voltage control in dq-reference frame.

condition. The MMC in Fig.1 can be operated as either a GFL-MMC or a GFM-MMC, depending on whether the MMC regulates its ac output current or voltage. The ac network in this context can be a passive grid (e.g., series-compensated grid, overhead lines) or an 'active' system dominated by power converters (e.g., offshore wind farm).

In a typical MMC-HVdc system, the GFL-MMC usually operates in dc-bus voltage control mode with a unity power factor, while the GFM-MMC works in single-loop ac voltage control mode. This work thus adopts MMC in these two control modes to demonstrate the passivity-based design of the wideband passivation control. Nevertheless, the proposed wideband passiviation control is also applicable to MMCs, even two-level VSCs, operating in other control modes. The parameters for the electrical system and the MMC controllers are tabulated in Tables I and II.

B. Simplified Impedance Model of MMCs

According to the small-signal impedance model proposed in [19], the small signal dynamics of MMC can be described

TABLE I
ELECTRICAL PARAMETERS OF MMC'S POWER STAGE [15]

Parameter	Symbol	Value	Unit
MMC rated power	P_N	900	MW
MMC rated ac voltage	U_N	300	kV RMS ph-ph
MMC rated dc voltage	V_{dcN}	$\pm$320	kV
Arm reactor	L_{arm}	50	mH
submodules per arm	N	200	N/A
submodule capacitance	C_{sm}	4.66	mF
time delay	e^{-sT_d}	200	μs

TABLE II
CONTROL PARAMETERS FOR GFL/GFM-MMC [15]

Controller	K_p	K_i	K_d
dc voltage control	0.0065	0.2	NA
ac current control	22.2	27915.5	7.85
circulating current control	22.2	13957.7	31.42
phase-locke loop	1.48×10^{-4}	0.0093	N/A
ac voltage control	0.5	54.4	N/A

as follows:

$$\begin{cases} \hat{\mathbf{v}}_{\mathbf{cu}}^{\mathbf{\Sigma}} = \mathbf{Z_c}(\mathbf{M_s}\hat{\mathbf{i}}_{\mathbf{u}} + \mathbf{I_u}\hat{\mathbf{m}}_{\mathbf{ac}}) \\ \mathbf{Z_l}\hat{\mathbf{i}}_{\mathbf{s}}/\mathbf{2} = \hat{\mathbf{v}}_{\mathbf{s}} + \mathbf{M_s}\hat{\mathbf{v}}_{\mathbf{cu}}^{\mathbf{\Sigma}} + \mathbf{V}_{\mathbf{cu}}^{\mathbf{\Sigma}}\hat{\mathbf{m}}_{\mathbf{s}} \end{cases} \tag{1}$$

where the $\hat{\mathbf{i}}_{\mathbf{s}}$, $\hat{\mathbf{v}}_{\mathbf{s}}$, $\hat{\mathbf{i}}_{\mathbf{u}}$, $\hat{\mathbf{m}}_{\mathbf{s}}$ and $\hat{\mathbf{v}}_{\mathbf{cu}}^{\mathbf{\Sigma}}$ denote the small-signal vectors of MMC output current, output voltage, upper arm current, modulation index, and sum capacitor voltages of the upper arm, respectively. $\mathbf{I_u}$, $\mathbf{M_s}$ and $\mathbf{V}_{\mathbf{cu}}^{\mathbf{\Sigma}}$ indicates corresponding steady-state components in the Toplitz matrix form. $\mathbf{Z_l}$ and $\mathbf{Z_c}$ represent the impedance matrix of the arm inductor and the module capacitor at small-signal frequencies. It is noteworthy that the propagation of small-signal perturbations in MMC output voltage (denoted as $\hat{v}_s(f_p)$) to sum capacitor voltages of SMs is primarily attenuated by: 1) arm reactors's admittance; and 2) SMs' capacitor impedance. Consequently, as small-signal perturbation frequency f_p approaches the second harmonic frequency and higher frequencies, the responses of $\hat{v}_{cu}^{\Sigma}(s)$ to $\hat{v}_s(f_p)$ become negligible [20]. This allows for the ignorance of $\hat{\mathbf{v}}_{\mathbf{cu}}^{\mathbf{\Sigma}}$ from (1). In addition, frequency coupling effects only affect the impedance shape of MMC and the corresponding system stability below the second harmonic frequency [21], [22]. Hence, (1) is simplified to

$$\frac{sL_{arm}}{2}\hat{i}_s(s) \overset{MF/HF}{\approx} \hat{v}_s(s) + NV_c^0\hat{m}_s(s) \tag{2}$$

where L_{arm} represents arm inductance, N is the number of SMs per arm and V_c^0 is the rated dc voltage of each SM capacitor, which is desired to be the same across all SMs if the SMs sorting algorithm is performed appropriately. As this paper focuses on reshaping MMC impedance from the second harmonic frequency above, where most of the control effect on MMC's impedance shape diminishes, several key points are made:

1) Similar to $\hat{\mathbf{v}}_{\mathbf{cu}}^{\mathbf{\Sigma}}$, the ac-side perturbation's propagation to small-signal responses in dc-side voltage is first attenuated by the arm inductor and SM capacitors, followed by the dc voltage controller (DVC) (Note: dc voltage controller are typically designed with relatively low bandwidth [11]).
2) Circulating current suppressing control (CCSC) and energy balancing control [23] are highly dependent on the dynamics of the sum of capacitor voltage $\hat{v}_{cu}^{\Sigma}$.
3) The response of Phase-locked loop (PLL) to the medium and high-frequency signals is considerably small due to the 2^{nd}-order low-pass structure of PLL's closed-loop transfer function.
4) Power controls and droop control can be ignored due to their low bandwidth [24]

Given these points, DVC, CCSC, and PLL can be ignored when modeling $\hat{m}_s(s)$ in (2).

When the MMC works in GFL mode, the ac current is regulated by the current control shown in Fig. 1(b), where $H_i(s)$ is the transfer function of the PI compensator for current control. K_d is current decoupling gain. Since I_s^{dq*} is 0 for $\hat{i}_s(s)$, $\hat{m}_s(s)$ generated by ac current control is given by

$$\hat{m}_s(s) = -\frac{1}{NV_c^0}H_i(s - j\omega_1)e^{-sT_d}\hat{i}_s(s) \tag{3}$$

where e^{-sT_d} represents the lumped time delay effect, and $-j\omega_1$ captures the fundamental frequency shift introduced by dq-transformation. Substituting (3) in (2) and rearranging it yields

$$Z_{p,GFL}(s) = \frac{\hat{v}_s(s)}{\hat{i}_s(s)} = sL_{eq} + e^{-sT_d}[H_i(s - j\omega_1) - jK_d] \tag{4}$$

where L_{eq} is half of the arm inductance. Similarly, when the MMC works in GFM mode, the ac voltage is regulated by voltage control shown in Fig. 1(c), in which $H_v(s)$ represents the PI compensator for voltage control. As a result, $\hat{m}_s(s)$ generated by ac voltage control is given as

$$\hat{m}_s(s) = -\frac{1}{NV_c^0}H_v(s - j\omega_1)e^{-sT_d}(-\hat{v}_s(s)) \tag{5}$$

Combining (5) and (2), the resulting simplified impedance of GFM-MMC can be expressed as

$$Z_{p,GFM}(s) = \frac{sL_{eq}}{1 + e^{-sT_d}H_v(s - j\omega_1)} \tag{6}$$

III. PASSIVITY-BASED DESIGN OF IMPEDANCE PASSIVATION CONTROL

A. Passivity-based Stability Analysis

The term "passive" has been used in the literature to describe the transfer function of an impedance (denoted as $Z(s)$) or admittance (denoted as $Y(s)$) with non-negative real part, and this property has been referred to as "passivity". A passive system is a guaranteed stable system since when the system is disturbed and moves away from the equilibrium point, it can return to the equilibrium point through the dissipation of energy [25]. However, it is rather hard to guarantee the passivity of MMC impedance across all frequencies. As a result, to enhance the stability of an MMC in a specific frequency range, one can reshape MMC impedance to be passive in that range. For example, in this work, the MMC impedance is expected to exhibit a passive characteristic above the second harmonic frequency to avoid any harmonic resonances.

The mathematical expression for a passive $Z(s)$ at frequency f is $\mathfrak{Re}\{Z(j2\pi f)\} \geq 0$, which is equivalent to $-\pi/2 \leq \angle Z(j2\pi f) \leq \pi/2$. Based on the passivity-based stability analysis [26], the stability of an interconnected system with MMC and ac network at frequency f can be guaranteed in two scenarios:

- When ac network is composed of *RLC* elements (i.e., $Z_g(j2\pi f)$ is passive), the system is stable when MMC impedance (denoted as $Z_p(j2\pi f)$) is passive.
- When ac network contains power converters with active control functions and $Z_g(j2\pi f)$ might have a negative real part, the system is stable when $Z_g(j2\pi f)+Z_p(j2\pi f)$ is passive.

For both scenarios, to prevent instability events of MMC at f, the MMC impedance should be designed as passive at f. One may ask in the second scenario, what if the MMC impedance (Z_p) is passive but the net impedance ($Z_g(s) + Z_p(s)$) is still negative. In such a condition, the system might need additional damping provided either from MMC side [15] or from grid side (e.g., apply the passivation method proposed in this work to power converters within the grid).

B. General Idea

Based on (4) and (6), without losing generality, the MMC impedance can be expressed in a general form given by

$$Z_p(s) = \frac{sL_{eq} + e^{-sT_d}G_i(s)}{1 + e^{-sT_d}G_v(s)} \tag{7}$$

where $G_i(s)$ represents the current feedback controller and $G_v(s)$ represents the voltage feedback or grid-voltage feedforward controller. When MMC works in open-loop control mode [27], $\hat{m}_s(s)$ in (2) becomes 0. As a consequence, $Z_p(s)$ in (7) degrades to a simple equivalent filter reactor sL_{eq}, no matter in the GFL or GFM mode, which is fully passive throughout the frequency range from the second harmonic frequency above. In such a condition, MMC is less risky for oscillation, especially when connected by passive networks, such as overhead transmission (OTL) and underground cables. However, since open-loop-controlled MMC lacks a feedback mechanism to adjust the output current and voltage according to changing system operating conditions or disturbances (e.g, ac-side voltage sag), such a control method cannot be used in practical systems. In order to retain closed-loop control of MMCs but maintain the $Z_p(s) = sL_{eq}$, it is necessary to use additional feedforward control functions to cancel out existing control loops, i.e. cancel out $G_i(s)$ and $G_v(s)$.

It is known that the use of current feedforward introduces a term to the numerator of the MMC impedance, while the use of voltage feedforward introduces a term to the denominator [15], thus the passivized impedance of an GFL-MMC and GFM-MMC are expressed as

$$Z_p^{PD}(s) = \frac{sL_{eq} + e^{-sT_d}G_i(s) + e^{-sT_d}y_i(s)}{1 + e^{-sT_d}G_v(s) + e^{-sT_d}y_v(s)} \tag{8}$$

with the superscript *PD* meaning "passivized", while $y_i(s)$ and $y_v(s)$ representing the transfer functions of the current feedforward and voltage feedforward controllers responsible for the impedance reshaping purpose, respectively.

1) $y_i(s)$ Cancel $G_i(s)$, $y_v(s)$ Cancel $G_v(s)$: The most straightforward scheme is using $y_i(s)$ to cancel current compensator $G_i(s)$ and using $y_v(s)$ to cancel voltage compensator $G_v(s)$, which yields $y_i(s) = -G_i(s)$ and $y_v(s) = -G_v(s)$. However, such a method also makes MMC lack of the feedback control mechanism especially for the regulation of fundamental components, thus has the same downside as open-loop control. A way to resolve this is to reconstruct the reference-tracking capability of current or voltage control by adding a transfer function to the forward path of the current or voltage controller, which is detailed in [17]. However, this reconstruction process requires an approximation of the ac current or voltage controller, which may affect the transient responses of the controller. Therefore, in this work, the passivation of the GFL-MMC via current feedforward and that of the GFM-MMC via the voltage feedforward are not further elaborated.

2) $y_i(s)$ Cancel $G_v(s)$, $y_v(s)$ Cancel $G_i(s)$: To reshape the output impedance of MMC to be a passive inductor while maintain the transient performance of the existing current or voltage control, a possible method is using $y_v(s)$ to equivalently cancel $G_i(s)$ and using $y_i(s)$ to equivalently cancel $G_v(s)$. By doing so, the time delay effect introduced to the MMC impedance through the current and voltage compensator is eliminated while the existing control function is retained. The detailed process to find the form (i.e, transfer function) of $y_i(s)$ and $y_v(s)$ will be presented in the sequel.

C. Passivity-based Design of Wideband Impedance Reshaping Control for GFL-MMC

1) Expression of the Passivation Term: Based on (4) and (8), the passivized GFL-MMC impedance can be expressed as

$$Z_{p,GFL}^{PD}(s) = \frac{sL_{eq} + e^{-sT_d}[H_i(s - j\omega_1) - jK_d]}{1 + e^{-sT_d}y_v(s)} \tag{9}$$

The voltage feedforward terms $y_v(s)$ for the passivation of the GFL-MMC can be obtained by solving

$$Z_{p,GFL}^{PD}(s) = \frac{sL_{eq} + e^{-sT_d}[H_i(s - j\omega_1) - jK_d]}{1 + e^{-sT_d}y_v(s)} = sL_{eq} \tag{10}$$

multiplying both sides of (10) with $[1 + e^{-sT_d}y_v(s)]$ and rearrange it, one can find out the expression of $y_v(s)$ as follows:

$$y_v(s) = \frac{1}{s}\left(\frac{K_{pi}}{L_{eq}} + \frac{K_{ii}}{L_{eq}}\frac{1}{s - j\omega_1} - j\frac{K_d}{L_{eq}}\right) \tag{11}$$

where K_{pi}, K_{ii} and K_d are the proportional gain, integral gain and dq-frame decoupling gain of the ac current controller in dq-reference frame, respectively. ω_1 is the fundamental frequency in rad/s. Based on Fig.1 and (11), the block diagram representation of the proposed passivation loop is depicted in Fig. 2, where $V_s(s)$ is the measured output voltage of the MMC, $M_d(s)$ is the modulation signal generated by the wideband passivation loop. It should be noted that current control can also be achieved by using the Proportional-Resonant (PR) controller, and to implement it one only needs to replace "G_i" in Fig. 2 by the PR compensator's structure.

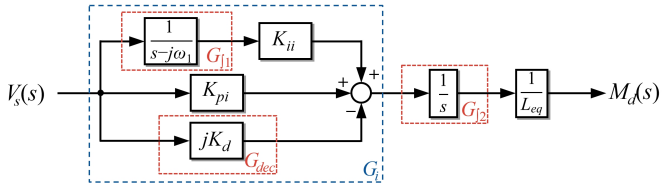

Fig. 2. Equivalent single-phase representation of the proposed wideband passviation loop for GFL-MMC

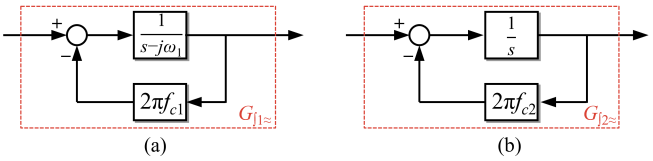

Fig. 3. Approximation of integrator in Fig. 2

As can be seen in Fig. 2, the passivation loop requires two integration parts, denoted as $G_{\int 1}$ and $G_{\int 2}$. $G_{\int 1}$ should be implemented in dq-reference frame to include the effect of the frequency shift (i.e., $s - j\omega_1$) and the reference angle of the dq transformation should be provided by the PLL, while $G_{\int 2}$ can be directly implemented in the phase domain. The transfer function G_{dec} can be regarded as the voltage decoupling gain, thus can be implemented in $\alpha\beta$ or dq reference frame. However, there are other modifications on the passivation loop based on practical considerations, as will be discussed next.

2) Practical Consideration on the Integration: The pure integrator cannot be directly realized in practical application for two primary reasons: 1) if the integration process initiates when the input voltage signals at certain frequency (not only the signal of interest) are not at their peak, a dc-offset will manifest in the output of passivation loop, which in turn appears in the output voltage of MMC. Note that, the level of the dc-offset is determined by the time instant the passivation loop is conducted; 2) integrator can amplify noise and drift over time due to its accumulating nature. This phenomenon coupled with a small dc-offset in voltage measurement can easily lead to saturation of the integrator and even instability of MMC [11].

Considering the feedback mechanism helps to correct any deviations of control input (e.g., like a dc-offset) and alters the integrator's response to avoid saturation, two pure integrators with negative feedback loop, as shown in Fig. 3 are used to replace $G_{\int 1}$ and $G_{\int 2}$ in Fig. 2. The transfer function of $G_{\int 1\approx}$ and $G_{\int 2\approx}$ are $1/(s+j2\pi f_{c1})$ and $1/(s+j2\pi f_{c2})$, where f_{c1} and f_{c2} can be regarded as the cutoff frequency of $G_{\int 1\approx}$ and $G_{\int 2\approx}$.

Remark 1: It is noteworthy that a smaller selection of the cutoff frequency of $1/(s + j2\pi f_c)$ yields a better approximation of the integrator, and thus provides a more effective wideband reshaping effect on the MMC impedance. However, the wideband passivation loop becomes more susceptible to dc offset in the MMC voltage measurement, and dc offset rejection duration becomes longer, which may affect the stability of MMC. In this work, f_{c1} and f_{c2} are designed to be 1 Hz. However, thanks to the feedback configuration shown in Fig. 3: 1) the selection of f_{c1} and f_{c2} can be made adaptive to the damping performance of MMC; 2) smooth startup can be ensured by setting a large value of f_c initially and gradually decreasing it, then sustaining it at 1 Hz.

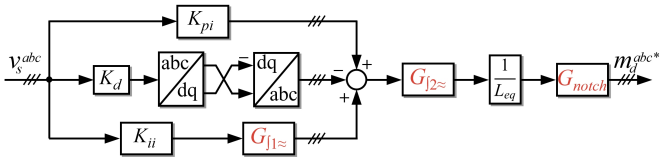

Fig. 4. Practical three-phase representation of the proposed wideband passviation loop for GFL-MMC

Remark 2: The reciprocal of (9) can be divided into $1/Z_{p,GFL}(s)$ and $e^{-sT_d}y_v(s)/Z_{p,GFL}(s)$. $1/Z_{p,GFL}(s)$ exhibits a positively damped inductive phase between 100 Hz and the cutoff frequency of the ac current control, while $e^{-sT_d}y_v(s)/Z_{p,GFL}(s)$ shows a capacitive phase characteristic. Therefore, when they are added together, the passivized impedance of MMC shows an inductive characteristic. If '$-j\omega_1$' in $y_v(s)$ is treated as an additional degree of freedom, it can be set to 0 to achieve the effect of providing additional positive damping to the GFL-MMC below the current control bandwidth. Note that, this modification does not deteriorate the passivation effect at frequencies higher than the current control bandwidth, as the difference between $(s - j2\pi f_1)$ and s becomes negligible above the current control bandwidth.

3) Notch Filter: Considering that the proposed passivation loop has a broadband impact on the MMC impedance, it might impact the current and voltage response at the fundamental frequency (e.g., the wideband passivation loop introduces additional grid-voltage feedforward). Therefore, a notch filter is needed to eliminate the impact of the wideband passivation loop at the fundamental frequency. The expression for the notch filter is given by

$$G_{notch}(s) = \frac{s^2 + \omega_1^2}{s^2 + \omega_c s + \omega_1^2} \tag{12}$$

where ω_c is the width of the rejected band of $G_{notch}(s)$ and ω_1 is the fundamental frequency, both in rad/s. To guarantee the notching effect also when fundamental frequency drift is in between $f_1 \pm 1$ Hz, ω_c is selected as 2π in this work.

4) Actual Representation of $y_v(s)$: The actual representation of $y_v(s)$ for the wideband passivation loop of GFL-MMC is given by

$$\tilde{y}_v(s) = G_{notch}(s)\frac{1}{s + j\omega_{c2}}\left(\frac{K_{pi}}{L_{eq}} + \frac{K_{ii}}{L_{eq}}\frac{1}{s + j\omega_{c1}} - j\frac{K_d}{L_{eq}}\right) \tag{13}$$

Based on (13) and all the discussion mentioned-above, the overall block diagram of the proposed wideband passivation loop is shown in Fig. 4 with subscript '$\int$' and '$\approx$' indicating integration and approximation, respectively. It should be noted that as the rejection band is selected to be very narrow around the fundamental frequency, thus it has negligible effect on impedance of MMC from the second harmonic frequency above.

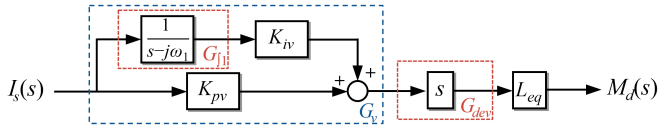

Fig. 5. Equivalent single-phase representation of the proposed wideband passviation loop for GFM-MMC

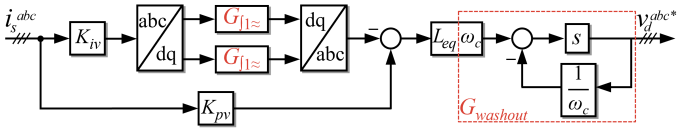

Fig. 6. Practical three-phase representation of the proposed wideband passviation loop for GFM-MMC

D. Passivity-based Design of Wideband Impedance Reshaping Control for GFM-MMC

1) Expression of Passivation Term: Similarly, based on (6) and (8), the passivized GFM-MMC impedance can be expressed as

$$Z_{p,GFM}^{PD}(s) = \frac{sL_{eq} + e^{-sT_d}y_i(s)}{1 + e^{-sT_d}H_v(s - j\omega_1)} \tag{14}$$

The current feedforward terms $y_i(s)$ for the passivation of the GFM-MMC can be obtained by solving the following equation

$$Z_{p,GFM}^{PD}(s) = \frac{sL_{eq} + e^{-sT_d}y_i(s)}{1 + e^{-sT_d}H_v(s - j\omega_1)} = sL_{eq} \tag{15}$$

multiplying both sides of (15) with $[1 + e^{-sT_d}H_v(s - j\omega_1)]$, one can find out the expression of $y_i(s)$ as follows.

$$y_i(s) = s\left(K_{pv}L_{eq} + \frac{K_{iv}L_{eq}}{s - j\omega_1}\right) \tag{16}$$

where K_{pv} and K_{iv} are the proportional gain and integral gain of the ac voltage compensator, respectively. ω_1 is the fundamental frequency in rad/s. Based on Fig. 1 and (16), the block diagram representation of the proposed passivation loop for GFM-MMC is depicted in Fig. 5, where $I_s(s)$ is the measured output current of the MMC, and $M_d(s)$ is the modulation signal generated by the proposed wideband passivation loop. It should be noted that voltage control can be achieved by PR compensator as well, and to implement it one only needs to replace "G_v" in Fig. 5 by the PR compensator's structure. Implementing $y_i(s)$ makes use of a derivative term G_{dev} and an integral term $1/(s - j\omega_1)$ in dq-reference frame. The reference angle $\theta(t)$ for the dq transformation is given directly by $2\pi f_g t$, where f_g is the fundamental frequency fixed by GFM-MMC.

2) Practical Consideration on the Integration: The consideration discussed in Sec. III-C regarding the practical consideration of integrator's implementation are worth reevaluating for the implementation of $y_i(s)$. Firstly, the approximation of integrator by the low-pass structure shown in Fig. 3 (a) is also applicable to the implementation of $y_i(s)$. On the other hand, one might wonder if it is feasible to substitute $1/s$ for $1/(s - j\omega_1)$ and then cancel it with s, thereby achieving a simple gain feedforward without using integrators. For the frequency above roughly 500 Hz, this approximation is acceptable. In the range between 100 and 500 Hz, the GFM-MMC impedance $Z_p(s)$ is a negatively damped inductive impedance, while $s/(s - j\omega_1)$ reveals a capacitive characteristic. Eliminating the term $1/(s - j\omega_1)$ would impact the effectiveness of the proposed passivation loop in this range, especially when the frequency approaches the second harmonic frequency. As a result, it is recommended to retain the frequency shift term in the implementation of $1/(s - j\omega_1)$. Note that the frequency shift can even be chosen slightly larger than ω_1 to enhance the passivation effect near the second harmonic frequency.

3) Practical Consideration on the Derivative Term: As can be seen from (16), $y_i(s)$ contains a pure derivative term s, which is approximated by a modified washout filter [28] in this work, as shown in (17), for several reasons: 1) it helps mitigate the amplification of measurement noises in current; 2) implementing a true derivative term later in a digital system can be challenging due to discretization errors and the need for high sampling rates; 3) a modified washout filter can be easily implemented in feedback form.

$$G_{washout}(s) = \frac{s}{1 + s/\omega_c} \tag{17}$$

4) Actual Representation of $y_i(s)$: It should be noted that the notch filter is not necessary in the implementation of $y_i(s)$ as the washout filter can inherently block the feedforward of the fundamental frequency component of MMC current. On the basis of the above discussion, the actual representation of $y_i(s)$ is given as

$$\tilde{y}_i(s) = \frac{s}{1 + s/\omega_c}\left(K_{pv}L_{eq} + \frac{K_{iv}L_{eq}}{s - j\omega_1}\right) \tag{18}$$

while its block diagram is depicted in Fig. 6. The modified washout filter is implemented using a feedback structure, which provides flexibility to adaptively regulate ω_c according to the damping requirement of the system and allows smooth conduction of the wideband passivation loop.

IV. Adaptive Passivation Based on Online Oscillation Detection

A. Rationale for Using Adaptive Control

Fig. 7 illustrates the block diagram of the current control with the proposed wideband passivation controller $\tilde{y}_v(s)$, based on which, the output current of GFL-MMC can be expressed by

$$i_s(s) = \underbrace{\frac{G_i(s)e^{-sT_d}}{G_i(s)e^{-sT_d} + sL_{eq}}}_{H_{cl}(s)} i_s^*(s) - \underbrace{\frac{1 + \tilde{y}_v(s)e^{-sT_d}}{G_i(s)e^{-sT_d} + sL_{eq}}}_{Y_{p,GFL}^{PD}(s)} v_s(s) \tag{19}$$

where $H_{cl}(s)$ is the closed-loop transfer function of the ac current $i_s(s)$ to the desired current reference i_s^*, while $Y_{p,GFL}^{PD}(s)$

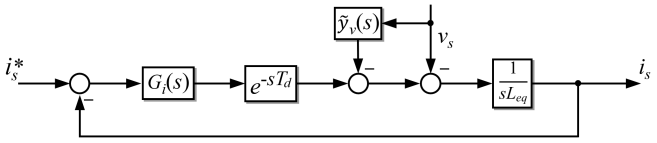

Fig. 7. Block diagram of closed-loop current control with $\tilde{y}_v(s)$ included

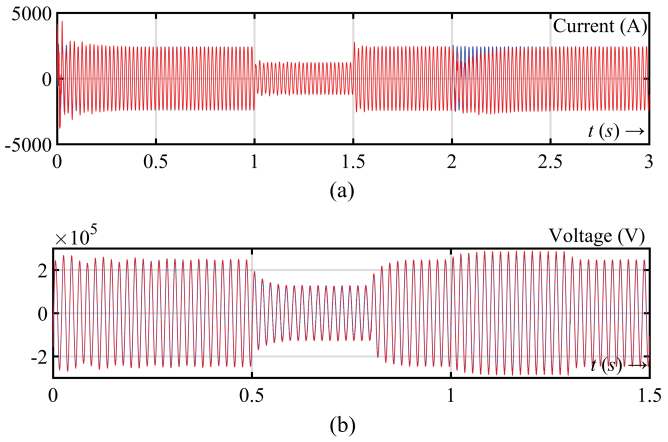

Fig. 8. (a) Simulated current responses of GFL-MMC with $\tilde{y}_v(s)$ (solid-red) and without $\tilde{y}_v(s)$ (solid-blue); (b) simulated voltage responses of GFM-MMC with $\tilde{y}_i(s)$ (solid-blue) and without $\tilde{y}_i(s)$ (solid-red)

is the admittance of GFL-MMC with proposed passivation loop. Thanks to the parallel structure between $\tilde{y}_v(s)$ and $G_i(s)$, the $\tilde{y}_v(s)$ has no impact on $H_{cl}(s)$, thus GFL-MMC retains its reference-tracking capability both before and after the wideband passivation loop is inserted. Similarly, the reference tracking capability of the ac voltage control can be retained for GFM-MMC when $\tilde{y}_i(s)$ is used to passivize its impedance. It is duly noted that the proposed impedance passivation method stands out because of two unique advantages over the method proposed in [17]:

- Since $H_{cl}(s)$ is not affected after the employment of the wideband passivation loop, the method avoids possible unwanted impacts arising from the approximation involved in reconstructing the transfer function in the feed-forward path (Note that, the unwanted impacts includes, but not limited to: 1) the inability to passivize MMC impedance between the second harmonic frequency and the current control bandwidth; 2) the slightly degraded reference tracking capability.).
- By avoiding structural modifications to existing controls and avoiding the need to apply it in advance, this approach facilitates the implementation of adaptive control strategies that will be elaborated on in the next section.

To evaluate reference-tracking capability, simulations of GFL(GFM)-MMC against an ideal voltage (current) source can be performed to verify current (voltage) responses, involving: 1) activating and disabling the passivation loop $\tilde{y}_v(s)$ ($\tilde{y}_i(s)$); 2) varying the current (voltage) control reference and comparing the corresponding response. Figure 8(a) illustrates the transient responses of the GFL-MMC's current, where the active power steps from 1 pu to 0.5 pu at $t = 1$ s and returns to 1 pu at $t = 1.5$ s. Similarly, Fig. 8(b) displays the voltage response of GFM-MMC, in which the d-axis voltage reference changes from 1 pu to 0.6 pu at $t = 0.5$ s and reverts to 1 pu at $t = 0.85$ s, while the q-axis voltage reference varies from 0 pu to 0.5 pu at $t = 1$ s and returns to 0 pu at $t = 1.3$ s. As depicted in Fig. 8, the transient performance of current (voltage) control for GFL(GFM)-MMC is maintained, indicating its advantages over existing wideband active damping methods. However, as can be seen from (19), $\tilde{y}_v(s)$ is added to the numerator of $Y^{PD}_{p,GFL}$, indicating that the current response of GFL-MMC would be affected by the passivation loop $\tilde{y}_v(s)$ during voltage disturbance. For a better understanding of this, Fig. 8(a) shows the current response ($i_s(s)$) of MMC when the grid voltage ($v_s(s)$) dips at $t = 2$s, with the current control reference i^*_s remains unchanged. As can be seen, the current response of the GFL-MMC with $\tilde{y}_v(s)$ exhibits a longer transient process after voltage dip when compared to the case of MMC without $\tilde{y}_v(s)$. As a result, although the passivation loop does not generally affect the MMC's transient performance, its continuous activation is not advisable. An alternative is the implementation of an adaptive control strategy based on online oscillation detection, which activates the passivation loop only when oscillations above the second harmonic frequency are detected. It is important to point out that, since the passivation loop reshapes the MMC impedance to be passive from the second-harmonic frequency above, there is no necessity to adjust it even when system resonance frequencies change due to alterations in ac network configurations and system operating conditions.

It is worth mentioning that, in terms of damping harmonic oscillations, the proposed wideband passivation loop can remain activated from the moment the MMC starts and throughout its operation. However, the adaptive control prevents wideband passivation loops from impacting the MMC's disturbance ride-through ability during normal steady-state operation. It should also be noted that the wideband impedance passivation method in [17] also impacts the current response GFL-MMC under voltage disturbance. However, it is not possible to integrate an adaptive control scheme into this method to avoid the impact of passivation, because the modifications must be made to the ac current control structure before the MMC can be operated.

B. Configuration of Adaptive Wideband Passivation

In contrast to adaptive narrowband damping methods that requires accurate estimation of oscillation frequency [13], [18], adaptive wideband passivation requires less precision in detection due to its broadband impedance reshaping effect. The online oscillation detection process, illustrated in Fig. 9(a), involves n_b buffers, each holding N samples. These samples are then smoothed by the Hanning window. The spacing (N_{hop}) and overlapping ($N_{overlap}$) samples between each window are configured to optimize the detection speed, as discussed in [18]. Fast Fourier transform (FFT) is applied to each window to obtain the spectrum of the measurement. A threshold set at 1% of the fundamental component is used to reject the noises. The decomposition of sequence components, performed in the frequency domain, mitigates the impact of phase imbalance in oscillations.

Fig. 9(b) shows the flowchart of the algorithm for identifying unstable oscillations using the denoised FFT spectrum. The algorithm extracts and compares the most significant spectral components within each window against a predetermined threshold, *Min* (5% of the fundamental component). If the amplitude of the extracted components in the latest window, denoted as $A_k(f_k)$, are all larger than *Min*, the algorithm verifies whether these components are consistent in frequency

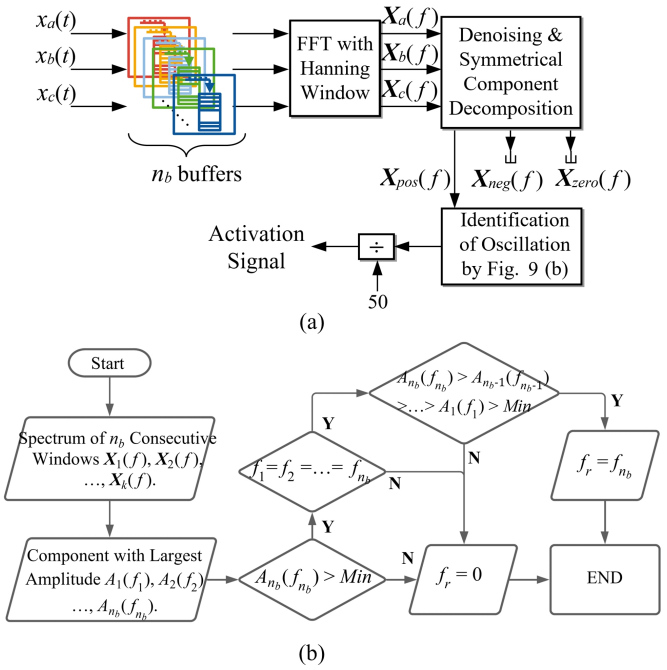

Fig. 9. (a) overall oscillation detection process; (b) flowchart depicting the algorithm for identification of oscillation frequency

and if their amplitude are in a growing manner. If so, the detection block will output the frequency f_{n_b}, which can also be used to activate the wideband passivation loop.

To minimize interference from power system transients, n_b, N, N_{hop} and $N_{overlap}$ should be carefully chosen. According to *IEEE Std 1159-2019* [29], most power system transients below 5 kHz vanish within 50 ms. Therefore, the minimum number of buffers, $n_{b_{min}}$, is set at 3 to prevent false identification system transients (e.g., MMC startup transient) as delay-induced oscillations. The window length, N, ensures the capture of a full oscillation cycle and is purposely selected to be an integer multiple of the fundamental period to avoid fundamental frequency bleeding due to aliasing. In this work, N is determined as f_s/f_1, balancing detection accuracy and speed, where f_s and f_1 are the sampling frequency and fundamental frequency, respectively. Spacing samples N_{hop} are selected to save computation memory and reduce false detection, while overlapping samples $N_{overlap}$ can be selected to enhance detection speed. However, both have to be carefully and properly selected to avoid mistaken detection. For example, if $(n_b N_{overlap}/f_s)$ is smaller than 0.1 ms, an impulsive transient would be identified as a growing oscillation during its rise time.

C. Robustness of Adaptive Wideband Impedance Passivation

For any damping control based on online oscillation detection, there are two important aspects for evaluating its robustness: 1) damping performance under inaccurate oscillation frequency detection; 2) damping effect on system stability when the system resonance conditions change (e.g., frequency change of resonances, disappearance of resonance, emergence of new resonances).

Unlike adaptive narrowband damping [14], [18], which targets a specific frequency, the impedance reshaping effect of the wideband passivation loop is not limited to a particular frequency (see Fig. 10). Once harmonic oscillation is detected, from the second harmonic frequency upward, the wideband passivation loop will completely eliminate the negative damping of MMC impedance and associated harmonic instability. As a result, the precision of oscillation frequency detection is not critical. It only requires that the presence of oscillations can be detected in order to activate the wideband passivation loop, without needing to know the exact oscillation frequency. In addition, since the effective frequency range is across entire range above the second harmonic frequency, once the wideband passivation loop is conducted, no new harmonic oscillations will occur regardless of how the system resonance conditions change. Hence, the proposed wideband impedance passivation loop minimizes its sensitivity under both aspects.

V. Validation and Performance Evaluation

This section presents frequency-domain analysis and time-domain numerical simulation results in MATLAB/Simulink to verify the wideband impedance passivation method developed in this work, and to demonstrate its applications to adaptive control of GFL-MMC and GFM-MMC through two case studies. The two case studies involve GFL-MMC connected to a long overhead transmission line and GFM-MMC connected by an offshore wind farm. The MMC and controller parameters used in this section are the same as those tabulated in Tables I and II.

Note that in this section, the passivation loop of GFL-MMC uses $\tilde{y}_v(s)$ expressed by (13), in which the ideal integrator is replaced by a low-pass filter with a bandwidth of 1 Hz. If a pure integrator is used, it will quickly saturate and destabilize the MMC. In contrast, in the validation of the passivation loop of GFM-MMC, $y_i(s)$ given by (16) is used, which does not cause instability in the numerical simulation. However, in practical applications, it is still recommended to use a high-pass filter for simulation, with the choice of bandwidth based on the approximation principles discussed in [30].

A. Impedance Verification

To verify the passivation effect of the proposed method on GFL-MMC impedance, Fig. 10(a) compares the analytical impedance responses of GFL-MMC with and without the passivation loop described in (13), in which the frequency scan results of each impedance response are also included for validation. As can be seen, the impedance of GFL-MMC is reshaped to be pure inductive (i.e., 90° phase response) with no negative damping from 100 Hz up. On the other hand, purposely removal of the frequency shift term of $G_{\int 1\approx}(s)$ and implementation of $G_{\int 1\approx}(s)$ directly in the phase domain reduce the passivation effect in the frequency range below 500 Hz, which keeps the phase response of MMC completely below 90°. In addition, the wideband passivation loop $\tilde{y}_v(s)$ levels up the magnitude dipping between 200 to 300 Hz from 20 dB to 30 dB, which makes the MMC less likely to interact with grid impedance, thereby further improving the system stability below 500 Hz. Similarly, to verify the passivation effect of the proposed method on GFM-MMC impedance, Fig. 10(b) compares the impedance responses of GFM-MMC with

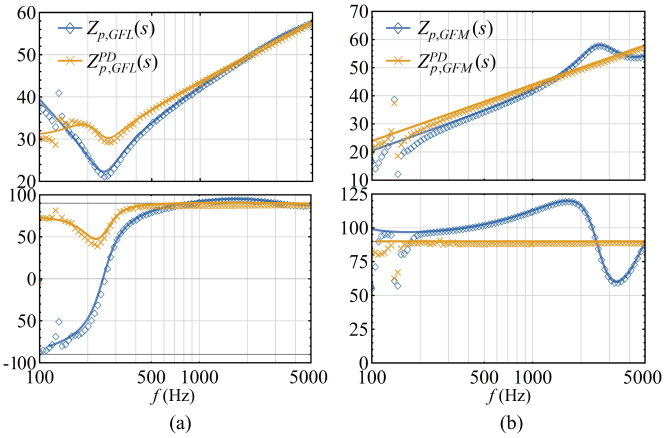

Fig. 10. Comparison of impedance response of: (a) GFL-MMC w/o $\tilde{y}_v(s)$ (blue) and GFL-MMC w/ $\tilde{y}_v(s)$ (yellow); (b) GFM-MMC w/o $\tilde{y}_i(s)$ (blue) and GFM-MMC w/ $y_i(s)$ (yellow); and their numerical scans (markers).

and without the passivation loop described in (16). It can be seen that the GFM-MMC impedance, by employing $y_i(s)$, is reshaped to be a passive reactance above the second harmonic frequency. As can also be seen from Fig. 10, the analytical responses closely match the frequency scan results in both cases, which further validate the effectiveness of the proposed method.

To further analyze the impact of the approximation of the integrator and derivative terms on the performance of wideband passivation. Fig. 11(a) plots the real part of $Z_{p,GFL}$(s) against $Z^{PD}_{p,GFL}$(s) passivized by $y_v(s)$ and $\tilde{y}_v(s)$, respectively; while Fig. 11(b) plots the real part of $Z_{p,GFM}$(s) against $Z^{PD}_{p,GFM}$(s) passivized by $y_i(s)$) and $\tilde{y}_i(s)$ (replacing pure derivative term by high-pass filter with bandwidth of 20 kHz, respectively.

It is evident that $y_v(s)$ and $y_i(s)$, the two ideal passivation loops, can completely eliminate the negative real part of the MMC impedance from 100 Hz above. Using $\tilde{y}_v(s)$ adds positive damping to the GFL-MMC impedance below 400 Hz, which ehances the passivity of MMC compared to the one using $y_v(s)$. However, due to the approximation of the pure integrator, $\tilde{y}_v(s)$ introduces a small negative damping to the MMC impedance between 450 Hz and 800 Hz. In contrast, the approximation of the pure derivative term by a 40 kHz high-pass filter can still completely eliminate the negative

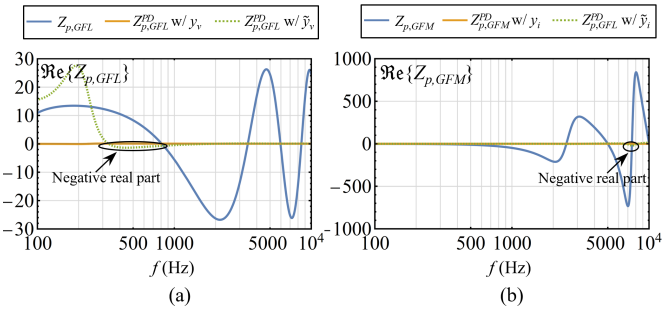

Fig. 11. Real part of impedance response of: (a) GFL-MMCs, in which f_c of low-pass filters in $\tilde{y}_v(s)$ is 1 Hz; (b) GFM-MMCs, in which f_c of high-pass filter in $\tilde{y}_i(s)$ is 40 kHz.

damping of the MMC impedance below the Nyquist frequency. However, it introduces negative damping between 6725 Hz and 8327 Hz, as pointed out by the black circle in Fig. 11. In practice, such a small amount of negative damping in these two cases could be compensated by the parasitic resistance of the passive network (e.g., transformer and overhead line/cable), thus less likely causing harmonic instability [10], [11].

In general, the passivized impedance responses of MMC (shown in Fig. 10) coupled with the transient performance evaluation of MMC (shown in Fig. 8), it is evident that the proposed wideband passivation can completely eliminate the negative damping of GFL-/GFM-MMC at and above the second harmonic frequency, without impacting the reference-tracking capability of existing controls.

B. Case 1: Wideband Passivation of GFL-MMC Impedance

The first case study is designed to validate the adaptive wideband passivation of GFL-MMC when it is connected to a long overhead transmission line (OTL), as shown in Fig. 12 where the OTL is modeled by the frequency-dependent model [31] in both analytical model and numerical simulation, while its parameter is tabulated in Table III (along with the offshore submarine cable parameters used in next case study). Figure 13 plots the impedance response of GFL-MMC without and with the proposed passivation loop $\tilde{y}_v(s)$, denoted as $Z_{p,GFL}(s)$ and $Z^{PD}_{p,GFL}(s)$, against the OTL impedance $Z_g(s)$, where $Z_{p,GFL}(s)$ forms five series resonance with $Z_g(s)$. The resonances at 1552, 2249 and 3371 Hz fall into the negative real-part region of $Z_{p,GFL}(s)$, where the system phase margin (PM) are $-2.3°$, $-0.4°$ and $5.5°$, respectively. As a result, there will be two oscillations at 1552 Hz and 2249 Hz when GFL-MMC connects to the OTL. The proposed passivation loop $\tilde{y}_v(s)$ totally removes the negative damping of GFL-MMC, and makes passivized MMC impedance form five series resonances with OTL impedance at 712, 1549, 2449, 3372, 4305 Hz, respectively. The PM at each resonance frequency is: $1.8°$, $1.94°$, $2.72°$, $5.5°$ and $7.72°$, indicating that the system is stable. It should be noted that, in the practical system, MMC arm, passive filter component and transformer at the point of common coupling (PCC), and the ac grid behind the OTL can further improve the phase margin by their parasitic resistances [11], [32].

To further validate the effectiveness of wideband passivation in mitigating medium- and high-frequency oscillations, as well

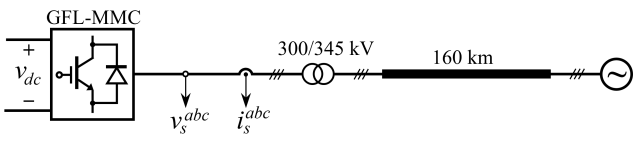

Fig. 12. GFL-MMC connected by 345kV/160-km overhead transmission.

TABLE III
PARAMETER OF AC TRANSMISSION

Parameter	Series Resistance	Series Inductance	Shunt Capacitance
Overhead Line	18.5×10^{-3} Ω/km	1×10^{-3} H/km	11.1×10^{-9} F/km
Offshore Cable	30×10^{-3} Ω/km	1.75×10^{-4} H/km	340×10^{-9} F/km

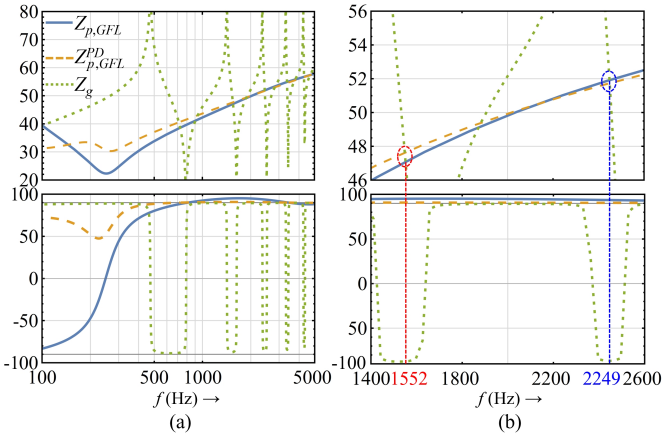

Fig. 13. Impedance response of: (a) GFL-MMC w/o $\tilde{y}_v(s)$ (solid blue) and GFL-MMC w/ $\tilde{y}_v(s)$ (dashed yellow) against OTL (dotted green); (b) zoom-in view of (a) between 1400 and 2600 Hz in linear frequency scale

TABLE IV
SETUP OF ONLINE OSCILLATION DETECTION IN CASE 1

Parameter	Symbol	Value	Unit
Analyzed # of windows	n_b	3	N/A
Sampling frequency	f_s	100	kHz
Window size of FF	N	2000	points
Overlapping-size of FFT	$N_{overlap}$	0	points
Detection Threshold	Min (current)	5% $\frac{\sqrt{2}}{\sqrt{3}}\frac{P_N}{U_N}$	Amp (A)

as the adaptive activation strategy of the passivation method, the simulated time-domain responses of GFL-MMC and the output of the oscillation detection unit are presented in Fig. 14. The setup of the online oscillation detection algorithm, as previously described in IV.B, is shown in Table IV. As

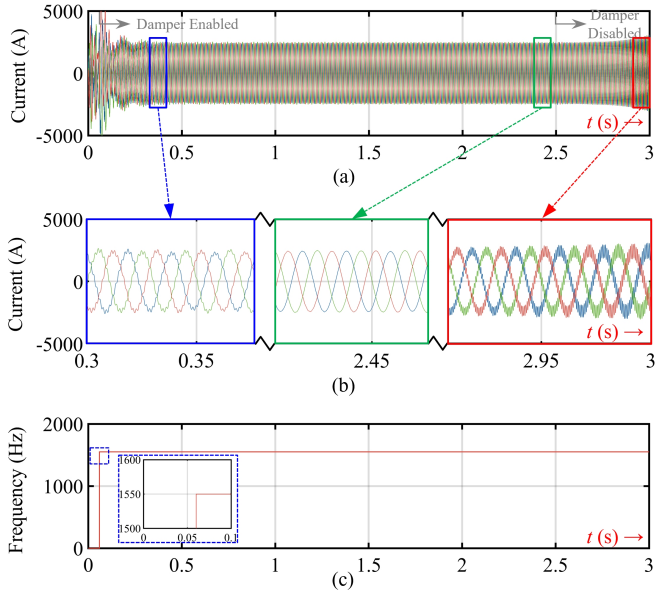

Fig. 14. simulated response of: (a) MMC output current; (b) MMC ouput current in three different time windows; (c) detected oscillation frequency

shown in Fig. 14(a), a large transient current is initiated when the MMC starts to connect to the OTL. This transient current naturally decays within two fundamental cycles and is not identified as an oscillation. With the decay of the transient, an oscillation at 1550 Hz is detected three fundamental cycles after the start-up of MMC, as indicated by the step-up change in signal shown in Fig. 14(c). Note that, the real oscillation frequency is 1552 Hz (See Fig. 13(b)). However, the number of samplings of FFT (N) is 2000, resulting in a frequency resolution of 50 Hz and a 2 Hz detection error. This 2 Hz error has no impact on the proposed wideband passivation method, because the method aims to eliminate the negative damping of MMC impedance across the entire frequency range above 100 Hz all at once, regardless of the specific frequencies where the oscillation events appear at. Subsequent to this detection, the wideband passivation loop is immediately activated, effectively suppressing the 1552 Hz oscillation and ensuring MMC's stable operation. Fig. 14(b) shows a zoom-in view of current responses during both oscillation mitigation and steady-state operation. At $t = 2.5$ s, the wideband passivation loop is purposely deactivated. By doing so, the negative PM of the system drives the 1552 Hz oscillation to grow again. Such a growing oscillation can clearly be observed in Fig. 14(b).

C. Case 2: Wideband Passivation of GFM-MMC Impedance

The second case illustrates the challenges associated with operating an offshore wind farm connected to MMC-HVDC and how the proposed approach overcomes them. The configuration of the offshore wind system is depicted in 15, where the offshore wind farm has a total capacity of 900 MW, and is organized into six parallel cable strings. At the end of each string, there is a wind park containing 10 wind turbines (WTs) of 15 MW rating each (e.g., Vestas® V236-15.0 MW™ [33]), which collectively produce 150 MW when operating at full power. Since the detailed model (i.e., switching-function-based VSC model) is used in MATLAB/Simulink to represent WT converters, the computation time and complexity of such a system is relatively large. Considering wind speed and wake effect deviations between WTs within a wind park are minimal [34], every 10 WT converters within the wind park are aggregated as a single 150 MW WT converter. In addition, since this paper is more focused on the stability issues at the point of common coupling (PCC) between the MMC and 66 kV cable collection bus, so the interactions among individual WTs at the end of each string can be ignored. This offshore wind system typically includes two types of delay-related oscillation issues in the frequency range above the second harmonic frequency:

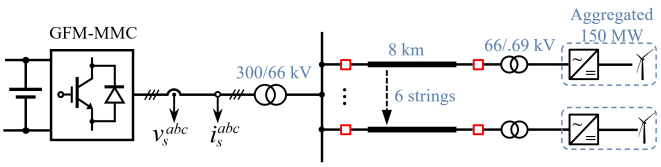

Fig. 15. GFM-MMC connected by offshore windfarm

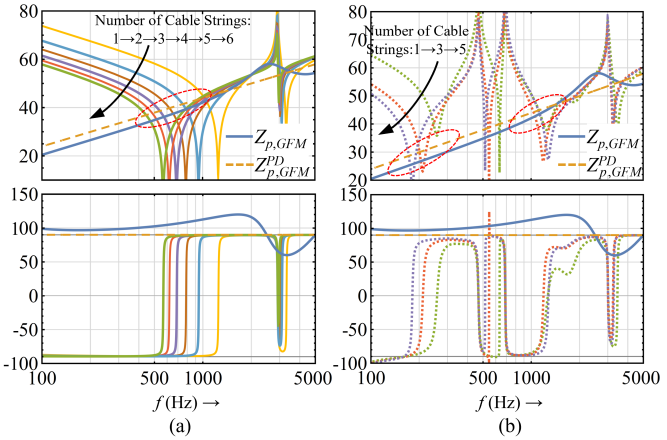

Fig. 16. Comparison of impedance response of GFM-MMC w/o $y_i(s)$ (solid blue) and w/ $y_i(s)$ (dashed yellow) against: (a) different cable strings; (b) different cable strings with aggregated turbines connected (dotted)

- The offshore cable strings needs to be energized before the startup of wind turbines, which makes GFM-MMC operates with only cable strings when turbines converters are not yet connected. Compared to long overhead lines, offshore cable strings has much less length, thus it virtually provides no positive damping to the MMC-cable system. In other words, if the GFM-MMC impedance exhibit even a light negative damping, the instability will immediately occurs in the system.
- After the turbines are running, the offshore wind farm impedance is dominated by turbine converters. The turbine converters may also shows the negative damped impedance characteristic due to time delay effect, thus the delay-induced oscillation can appear between GFM-MMC and offshore wind turbines.

To better explain the two types of oscillations, Fig. 16 compares the impedance response of GFM-MMC and wind farm with that of different ac network configuration. As can be seen from Fig. 16(a), regardless of the number of stings connected to the MMC, the PM of the MMC-cable system at the intersection frequency is always negative. The most severe condition occurs when only one cable string is connected, yielding a PM of $-22°$ at 1055 Hz. Using the proposed wideband passivation loop $y_i(s)$, the GFM-MMC is passivized to be an equivalent arm inductor from 100 Hz above. As the number of cable strings increases from 1 to 6, the magnitude intersections locate at 1023 Hz (1 string), 752 Hz (2 strings), 621 Hz (3 strings), 541 Hz (4 strings), 486 Hz (5 strings), and 445 Hz (6 string). The corresponding PMs at these intersections are $1.4°$, $1.13°$, $1.1°$, $1.11°$, $1.13°$ and $3.17°$, respectively. As a result, with the activation of the passivation loop $y_i(s)$, no instability issues should arise during the energization of the cable network.

Upon energization of the cable network, the impedance of the ac network changes based on the number of turbines connected to the cable network. Fig. 16(b) illustrates the impedance responses of the wind farm with 1, 3 and 5 strings, each connected by a 150 MW turbine, compared against the impedance response of GFM-MMC with and without the proposed passivation loop $y_i(s)$. As depicted in Fig. 16(b),

TABLE V
SETUP OF ONLINE OSCILLATION DETECTION IN CASE 2

Parameter	Symbol	Value	Unit
Analyzed # of windows	n_b	3	N/A
Sampling frequency	f_s	100	kHz
Window size of FFT	N	2000	points
Overlapping-size of FFT	$N_{overlap}$	1900	points
Detection Threshold	Min	5% $\frac{\sqrt{2}}{\sqrt{3}}U_N$	Volt (V)

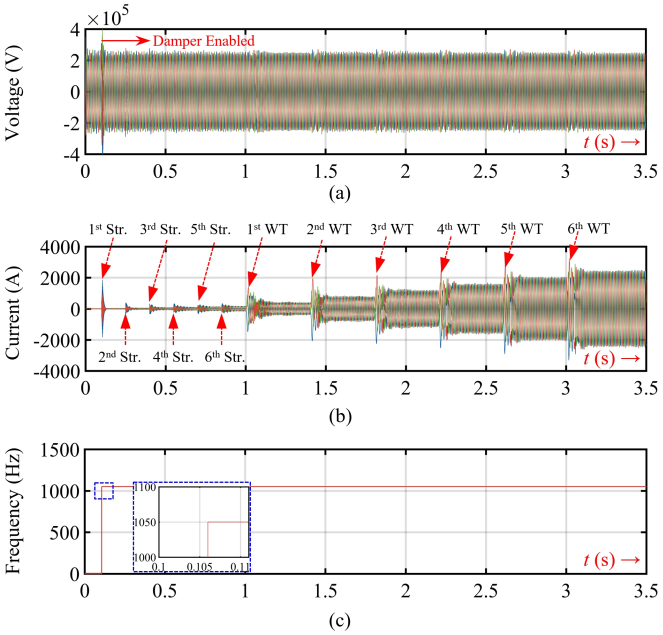

Fig. 17. simulated output response of (a) GFM-MMC current; (b) GFM-MMC voltage, and (c) detected oscillation frequency

with a single string connected by a 150 MW turbine, the GFM-MMC impedance intersects with the wind farm impedance at 1135 Hz, where the PM is $-5.91°$. Connecting three 150 MW turbines to three strings moves the resonance frequency to 1056 Hz, and significantly reduces the PM to $-17.78°$. With five strings connected by aggregated turbines, the resonance frequency shifts to 1128 Hz, where the PM is further jeopardized to $-19.25°$. In addition, a medium frequency oscillation is developed at 175 Hz, with a PM of $-1.51°$. In contrast, the negative damping of GFM-MMC is completely eliminated by the proposed passivation loop $y_i(s)$, compensating all negative PMs to positive values. As an example, in the case of a single string, the resonance frequency shifts from 1135 Hz to 1115 Hz, but largely increasing the PM to $15.23°$. Therefore, the wind farm is expected to be stably integrated into the GFM-MMC once the turbines are up and running.

The simulated response of GFM-MMC during the cable energization and wind integration process is shown in Fig. 17(a) and (b), while the online oscillation detection output is shown in Fig. 17(c). The setup of the online oscillation detection algorithm, as previously described in IV.B, is shown in Table V. Note that, the PM between GFM-MMC and a single string is $-22°$, indicating a fast-growing oscillation. To

ensure prompt detection of this unstable oscillation, N_{ovelap} is selected as 95% of N. The energization of the first cable string is performed at $t = 0.1$ s, the 1023 Hz oscillation is immediate and unstable, and it is detected within 0.006 s, as indicated by the step-up change of the signal shown in Fig. 17(c). The wideband passivation loop $y_i(s)$ is then activated, and the 1023 Hz oscillation is immediately mitigated, allowing the rest of the cable strings to be connected. Thanks to $y_i(s)$, no oscillation event occurs during the subsequent cable energization process and while the turbine converters are connected to the GFM-MMC.

VI. Conclusion and Future Work

This paper presented a wideband impedance passivation loop and its design consideration. By feedforwarding MMC current and voltage through the passivation loop, the proposed impedance passivation approach equivalently cancels out the existing ac current/voltage control and time delay effect on MMC impedance, while retaining the reference-tracking capability of the existing controls. Therefore, time-delay-induced negative damping of the MMC impedance and associated harmonic instability is completely eliminated. Important considerations of the proposed method lay on: 1) practical implementation of the proposed wideband impedance passivation loop; 2) adaptive control to maintain disturbance ride-through capability during steady-state operation of MMC. Two case studies demonstrate the use and effectiveness of the proposed wideband impedance passivation method in solving harmonic oscillations in two typical MMC-HVdc systems.

A future work will analyze how wideband passivation loop affect MMC impedance characteristic in the low-frequency range. There are a few points to be considered when analyzing the impact: 1) Full impedance models of MMC is required to capture complete dynamics of MMC; 2) It is necessary to model the impedance of MMC operated in different control modes separately, and to analyze the impact of wideband passivation loops to them in the low-frequency range respectively; 3) Frequency coupling effect of MMC impedance should be considered during the analysis.

References

[1] Y. Cheng and *et al.*, "Real-world subsynchronous oscillation events in power grids with high penetrations of inverter-based resources," *IEEE Transactions on Power Systems*, vol. 38, no. 1, pp. 316–330, 2023.

[2] J. Lyu, X. Zhang, X. Cai, and M. Molinas, "Harmonic state-space based small-signal impedance modeling of a modular multilevel converter with consideration of internal harmonic dynamics," *IEEE Transactions on Power Electronics*, vol. 34, no. 3, pp. 2134–2148, 2019.

[3] H. Li, J. Shair, J. Zhang, and X. Xie, "Investigation of subsynchronous oscillation in a dfig-based wind power plant connected to mtdc grid," *IEEE Transactions on Power Systems*, vol. 38, no. 4, pp. 3222–3231, 2023.

[4] W. Yan and *et al.*, "On the low risk of ssr in type iii wind turbines operating with grid-forming control," *IEEE Transactions on Sustainable Energy*, vol. 15, no. 1, pp. 443–453, 2024.

[5] H. Saad, Y. Fillion, S. Deschanvres, Y. Vernay, and S. Dennetière, "On resonances and harmonics in HVDC-MMC station connected to ac grid," *IEEE Transactions on Power Delivery*, vol. 32, pp. 1565–1573, January 2017.

[6] C. Zou and *et al.*, "Analysis of resonance between a VSC-HVDC converter and the ac grid," *IEEE Transactions on Power Electronics*, vol. 33, pp. 10157–10168, February 2018.

[7] Y. Li, T. An, D. Zhang, X. Pei, K. Ji, and G. Tang, "Analysis and suppression control of high frequency resonance for MMC-HVDC system," *IEEE Transactions on Power Delivery*, vol. 36, no. 6, pp. 3867–3881, 2021.

[8] H. Lin, T. Xue, J. Lyu, and X. Cai, "Impact of different ac voltage control modes of wind-farm-side mmc on stability of mmc-hvdc with offshore wind farms," *Journal of Modern Power Systems and Clean Energy*, vol. 11, no. 5, pp. 1687–1699, 2023.

[9] G. Li, H. Ye, and Z. Bin, "High-frequency oscillation mechanism analysis of wind farm-side mmc station considering converter transformer stray capacitance," *International Journal of Electrical Power & Energy Systems*, vol. 153, p. 109179, 2023.

[10] L. Harnefors, R. Finger, X. Wang, H. Bai, and F. Blaabjerg, "Vsc input-admittance modeling and analysis above the nyquist frequency for passivity-based stability assessment," *IEEE Transactions on Industrial Electronics*, vol. 64, no. 8, pp. 6362–6370, 2017.

[11] H. Wu and X. Wang, "Virtual-flux-based passivation of current control for grid-connected VSCs," *IEEE Transactions on Power Electronics*, vol. 35, pp. 12673–12677, December 2020.

[12] K. Ji, W. Chen, X. Wu, H. Pang, J. Hu, S. Liu, F. Cheng, and G. Tang, "High frequency stability constraints based mmc controller design using nsga-iii algorithm," *CSEE Journal of Power and Energy Systems*, vol. 9, no. 2, pp. 623–633, 2023.

[13] X. Wang, F. Blaabjerg, and M. Liserre, "An active damper to suppress multiple resonances with unknown frequencies," in *2014 IEEE Applied Power Electronics Conference and Exposition - APEC 2014*, pp. 2184–2191, 2014.

[14] J. Man, L. Chen, V. Terzija, and X. Xie, "Mitigating high-frequency resonance in MMC-HVDC systems using adaptive notch filters," *IEEE Transactions on Power Systems*, pp. 1–1, 2021.

[15] P. Huang and L. Vanfretti, "Multi-tuned narrowband damping for suppressing mmc high-frequency oscillations," *IEEE Transactions on Power Delivery*, vol. 38, no. 6, pp. 3804–3819, 2023.

[16] T. Joseph, C. E. Ugalde-Loo, S. Balasubramaniam, J. Liang, and G. Li, "Experimental validation of an active wideband ssr damping scheme for series-compensated networks," *IEEE Transactions on Power Delivery*, vol. 35, no. 1, pp. 58–70, 2020.

[17] H. Wu and X. Wang, "Passivity-based dual-loop vector voltage and current control for grid-forming VSCs," *IEEE Trans. Power Electron.*, vol. 36, pp. 8647–8652, Aug. 2021.

[18] P. Huang and L. Vanfretti, "Adaptive damping control of mmc to suppress high-frequency resonance," *IEEE Transactions on Industry Applications*, vol. 59, no. 6, pp. 7224–7237, 2023.

[19] J. Sun and H. Liu, "Sequence impedance modeling of modular multilevel converters," *IEEE Journal of Emerging and Selected Topics in Power Electronics*, vol. 5, no. 4, pp. 1427–1443, 2017.

[20] H. Wu, X. Wang, and L. H. Kocewiak, "Impedance-based stability analysis of voltage-controlled mmcs feeding linear ac systems," *IEEE Journal of Emerging and Selected Topics in Power Electronics*, vol. 8, no. 4, pp. 4060–4074, 2020.

[21] S. Shah, P. Koralewicz, V. Gevorgian, and R. Wallen, "Sequence impedance measurement of utility-scale wind turbines and inverters – reference frame, frequency coupling, and mimo/siso forms," *IEEE Transactions on Energy Conversion*, vol. 37, no. 1, pp. 75–86, 2022.

[22] S. Shah, P. Koralewicz, V. Gevorgian, and L. Parsa, "Small-signal modeling and design of phase-locked loops using harmonic signal-flow graphs," *IEEE Transactions on Energy Conversion*, vol. 35, no. 2, pp. 600–610, 2020.

[23] P. Huang and L. Vanfretti, "Analysis of internal energy in GFL-MMCs and a decoupled energy control scheme," in *2023 IEEE Power & Energy Society Innovative Smart Grid Technologies Conference (ISGT)*, pp. 1–5, 2023.

[24] W. Yan, S. Shah, V. Gevorgian, P. Koralewicz, R. Wallen, and D. W. Gao, "On the low risk of ssr in type iii wind turbines operating with grid-forming control," *IEEE Transactions on Sustainable Energy*, vol. 15, no. 1, pp. 443–453, 2024.

[25] J. C. Willems, "Dissipative dynamical systems part i: General theory," *Archive for Rational Mechanics and Analysis*, vol. 45, pp. 321–351, 1972.

[26] A. J. Agbemuko, J. L. Domínguez-García, O. Gomis-Bellmunt, and L. Harnefors, "Passivity-based analysis and performance enhancement of a vector controlled vsc connected to a weak ac grid," *IEEE Transactions on Power Delivery*, vol. 36, no. 1, pp. 156–167, 2021.

[27] L. Angquist, A. Antonopoulos, D. Siemaszko, K. Ilves, M. Vasiladiotis, and H.-P. Nee, "Open-loop control of modular multilevel converters using estimation of stored energy," *IEEE Transactions on Industry Applications*, vol. 47, no. 6, pp. 2516–2524, 2011.

[28] H. A. Mohammadpour and E. Santi, "Ssr damping controller design and optimal placement in rotor-side and grid-side converters of series-compensated dfig-based wind farm," *IEEE Transactions on Sustainable Energy*, vol. 6, no. 2, pp. 388–399, 2015.
[29] "IEEE recommended practice for monitoring electric power quality,," *IEEE Std 1159-2019 (Revision of IEEE Std 1159-2009)*, pp. 1–98, 2019.
[30] L. Harnefors, A. G. Yepes, A. Vidal, and J. Doval-Gandoy, "Passivity-based controller design of grid-connected VSCs for prevention of electrical resonance instability," *IEEE Transactions on Industrial Electronics*, vol. 62, no. 2, pp. 702–710, 2015.
[31] J. R. Marti, "Accurate modelling of frequency-dependent transmission lines in electromagnetic transient simulations," *IEEE Transactions on Power Apparatus and Systems*, vol. PAS-101, no. 1, pp. 147–157, 1982.
[32] P. Huang and L. Vanfretti, "Mitigation of mmc high-frequency oscillations by wideband passivation," in *2023 IEEE Kansas Power and Energy Conference (KPEC)*, pp. 1–6, 2023.
[33] G. E. Barter, L. Sethuraman, P. Bortolotti, J. Keller, and D. A. Torrey, "Beyond 15 mw: A cost of energy perspective on the next generation of drivetrain technologies for offshore wind turbines," *Applied Energy*, vol. 344, p. 121272, 2023.
[34] M. Poeller and S. Achilles, "Aggregated wind park models for analysing power system dynamics," Nov 2003.

Pengxiang Huang (Member, IEEE) received the B.S. degree from the Shanghai University of Electric Power, Shanghai, China, in 2015, the M.S. degree from George Washington University (GWU), Washington, DC, USA, in 2018, and the Ph.D. degree from Rensselaer Polytechnic Institute (RPI), Troy, NY, USA, in 2023, all in electrical engineering. He is currently a Research Engineer with the National Renewable Energy Laboratory (NREL) in Golden, CO, USA. His research interests include the fields linked with renewable energy integration, VSC-based HVDC systems and flexible ac transmission system.

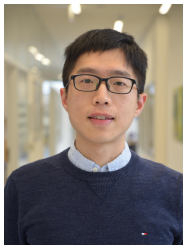

Heng Wu (Senior Member, IEEE) received B.S. and M.S. degrees in electrical engineering from Nanjing University of Aeronautics and Astronautics (NUAA), Nanjing, China, in 2012 and 2015, respectively, and the Ph.D. degree in electrical engineering from Aalborg University, Aalborg, Denmark, in 2020. He is now an Assistant Professor and Leader of Electronic Power Grid (eGRID) Research Group with AAU Energy, Aalborg University.

Luigi Vanfretti Luigi Vanfretti (Senior Member, IEEE) was born in Guatemala and obtained his Engineering Degree with a concentration in Electrical Power in 2005 from Universidad de San Carlos de Guatemala. He then received the M.Sc. and Ph.D. degrees in electric power engineering from the Rensselaer Polytechnic Institute (RPI), Troy, NY, USA, in 2007 and 2009, respectively. He held postdoctoral research posts both at RPI and KTH Royal Institute of Technology, Sweden, in 2010.

He is currently a Full Professor at Rensselaer Polytechnic Institute, since July 2022, where he was a tenured Associate Professor from 2017-6/2022-6. At RPI, he leads research projects in his laboratory and with his research team, ALSETLab, in the domains of electrical power systems and aircraft electrification.

Oriol Gomis-Bellmunt (S'05-M'07-SM'12-F'21) received the degree in industrial engineering from the School of Industrial Engineering of Barcelona (ETSEIB), Technical University of Catalonia (UPC), Barcelona, Spain, in 2001 and the Ph.D. degree in electrical engineering from the UPC in 2007. In 1999, he joined Engitrol S.L. where he worked as Project Engineer in the automation and control industry. Since 2004, he has been with the Electrical Engineering Department, UPC where he is a Professor and participates in the CITCEA-UPC Research Group. Since 2020, he is an ICREA Academia researcher. In 2022, he co-founded the start-up eRoots Analytics focused on the analysis of modern power systems. His research interests include the fields linked with power electronics, power systems and renewable energy integration in power systems.